Advanced 64 Cu/67 Cu-Based Theranostics: Application of the Copper Chelator TE1PA to a Murine Model of HER2-positive Gastric Cancer

Julie Pineau, Cédric Ollier, Céline Mothes, Sarah Belderbos, Nathalie Le Bris, Raphaël Tripier

Advanced ^{64}Cu/^{67}Cu-Based Theranostics: Application of the Copper Chelator TE1PA to a Murine Model of HER2-positive Gastric Cancer

Julie Pineau,[a] Cédric Ollier,[a] Céline Mothes,[b] Sarah Belderbos,[b] Nathalie Le Bris,[a],* and Raphaël Tripier,[a],*

[a] Univ Brest, UMR CNRS 6521 CEMCA, 6 avenue Victor le Gorgeu, 29238 Brest, France. Emails: raphael.tripier@univ-brest.fr; nathalie.lebris@univ-brest.fr

[b] Oncodesign Services, 20 rue Jean Mazen, 21000 Dijon, France

KEYWORDS. Bifunctional TE1PA • Theranostic • PET imaging • Copper-64/67 • Trastuzumab • Gastric cancer

ABSTRACT: The development of ^{64}Cu/^{67}Cu-based theranostic probes addresses the need for integrated cancer diagnosis and therapy. To target HER2-positive gastric cancer, trastuzumab was conjugated to ***p*-SCN-Bn-TE1PA** (DOL of 1.1–2.0), achieving high yields and purity. Binding assays on BT-474 cells confirmed the preserved cellular uptake of the bioconjugate. The successful radiolabeling of **Trastuzumab-*p*-SCN-Bn-TE1PA** (DOL of 2) with both the ^{64}Cu- and ^{67}Cu-isotopes demonstrated suitability for *in vivo* studies. In a preclinical model of HER2-positive gastric cancer, [^{64}Cu]Cu-**Trastuzumab-*p*-SCN-Bn-TE1PA** enabled effective PET imaging with tumor-specific uptake (> 21%IA/g) and clearance through the spleen, liver and kidneys. Therapeutic studies with [^{67}Cu]Cu **Trastuzumab-*p*-SCN-BnTE1PA** (10–20 MBq) demonstrated dose-dependent tumor inhibition of growth, without toxicity or adverse health effects. This work exemplifies the clinical potential of associating ^{64}Cu-imaging and ^{67}Cu-therapy. By combining a robust isotopic pair, a customized bifunctional chelator and trastuzumab, this study demonstrates a promising approach for HER2-positive gastric cancer treatment in nuclear medicine, paving the way for personalized copper-based theranostics.

INTRODUCTION

Human epidermal growth factor receptor 2 (HER2) is overexpressed in several cancers,[1] including breast, ovarian, prostate, lung, esophageal and gastric cancers.[2] Among these, gastric cancer is one the most prevalent and lethal. Often diagnosed at an advanced stage, it has limited treatment options and is associated with poor prognosis. HER2-targeting drugs, such as trastuzumab and pertuzumab, have shown efficacy in treating HER2-positive gastric cancer, offering improved outcomes than traditional chemotherapy.[3] Trastuzumab, the first FDA-approved HER2-targeting agent, plays a crucial role in treatment. However, accurate validation of HER2 expression in primary tumors and metastatic sites is essential for effective therapy.

Over the last few decades, nuclear medicine has revolutionized oncology, for the diagnosis and treatment of cancer. Radiopharmaceuticals used in positron emission tomography (PET) have become vital tools for identifying patients likely to respond to targeted therapies and for monitoring treatment response.[4] PET imaging using radionuclide chelation offers several advantages over conventional PET using fluorine-18 or carbon-11, such as improved chemical stability, increased selectivity and enhanced molecular imaging. Researchers have developed imaging probes based on radiolabeled antibodies derived from trastuzumab for non-invasive assessment of HER2 expression. These advanced molecular imaging techniques are invaluable for optimizing therapy timing, monitoring treatment response, and detecting metastases. Obviously, therapy remains the ultimate goal, and the combination of diagnostic imaging and therapy interventions, a concept known as "theranostics", has gained prominence. Theranostics typically involve radiopharmaceuticals, compounds labeled with radioactive isotopes, that enable both imaging and therapy. A chelating agent allows the use of different radionuclides for either purpose, enabling personalized treatment strategies tailored to the patient's unique tumor biology.[5]

In neuroendocrine tumors, for instance, [^{68}Ga]Ga-DOTA-TATE has been used for theranostic PET imaging prior to radiotherapy with [^{177}Lu]Lu-DOTA-TATE (Lutathera®).[6] However, limitations include the short half-life of gallium-68 (~68 min), which restricts its use for long-term imaging, and the need for an on-site generator for its preparation. Furthermore, differences between gallium and lutetium elements in terms of size and stability lead to the production of radiopharmaceuticals with distinct properties, affecting the location and retention of the final compound. Additionally, DOTA-TATE based radiopharmaceuticals are applicable only to neuroendocrine tumors,[7] which limits their use for other cancers, such as gastric cancer. The use of the same element for both imaging and therapy represents a significant advancement in radionuclide therapy. Two copper radionuclides, copper-64 and copper-67 form a matched theranostic pair.[8,9,10] Copper-64 (β^+ 17.9%, $E_{\beta+\,(mean)}$ = 278 keV) is a positron emitter, with a half-life of 12.7 hours, well-suited for PET imaging, while copper-67 (β^- 100%, $E_{\beta-\,(mean)}$ = 141 keV), with a half-life of 61.9 hours, emits β^- particles ideal for treating small tumors and metastatic disease. Recent advancements in copper chelator development and production methods have renewed interest in copper-67.[11] Importantly, copper-67 has also demonstrated its usefulness from a diagnostic standpoint thanks to its gamma emissions.[12]

The effective use of copper radionuclides in radiopharmaceuticals requires chelators capable of forming very stable complexes *in vivo*. We have shown that **TE1PA**, a cyclam-based

ligand with a pendant picolinate arm, forms a copper(II) complex with exceptional thermodynamic and kinetic stability *in vivo* surpassing previously reported chelators.[13] This high stability is due to the overall architecture of the complex. Even though the carboxylate pendant arm is not directly involved in coordination with the copper center, it plays an important structural role by contributing to the preorganization of the ligand. This preorganization facilitates rapid complexation kinetics at room temperature, which is particularly favorable for antibody-based radiopharmaceuticals. In the resulting complex, an intramolecular hydrogen bond is observed (see X-ray structures of the Cu^{2+} complexes in Figure 1), which further contributes to the high thermodynamic and kinetic inertness of the complex. These properties subsequently led to extensive *in vitro* and *in vivo* studies with copper-64. The resulting radiocomplex exhibits excellent stability and efficient clearance, especially compared with DOTA, which shows significant dissociation *in vivo*, particularly in the liver, due to competition with superoxide dismutase (SOD).[14]

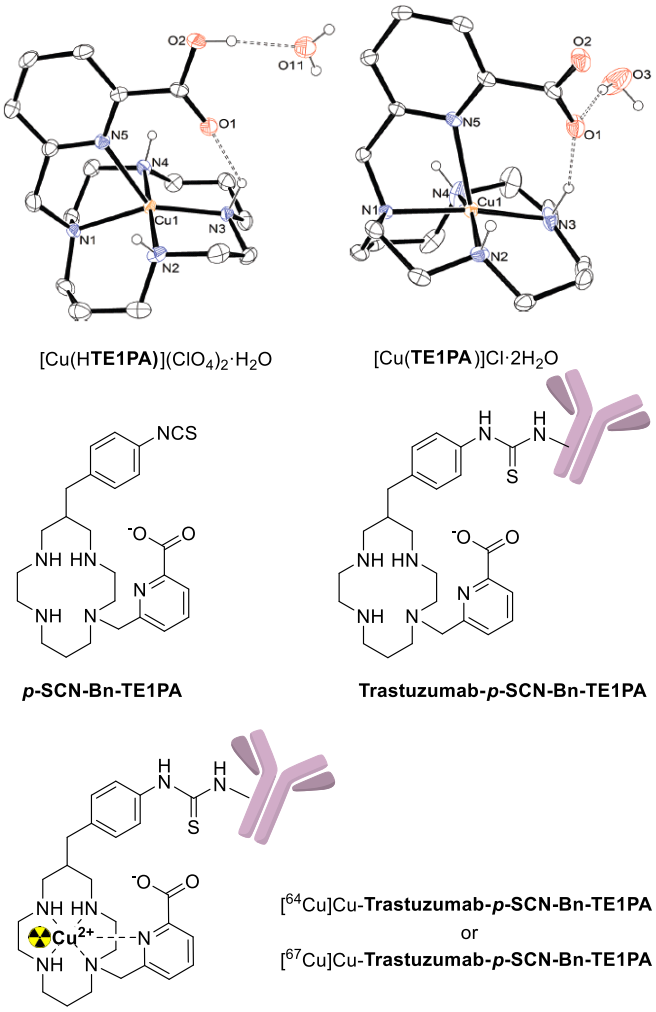

Figure 1. Bifunctional chelator, bioconjugate and radiopharmaceutical derived from the TE1PA chelator studied in this work.

TE1PA was further modified into a bifunctional chelator, ***p*-SCN-Bn-TE1PA** (Figure 1), allowing its conjugation to biological vectors that target specific cells or tissues. When conjugated to the rat antibody 9E7.4, specific to CD138 (overexpressed on multiple myeloma cells), ***p*-SCN-Bn-TE1PA** showed superior targeting efficiency and stability compared to its DOTA or NOTA-based analogues.[15,16]

Building on these advances, the approach was extended to HER2-positive gastric cancer by conjugating ***p*-SCN-Bn-TE1PA** with trastuzumab, resulting in **Trastuzumab-*p*-SCN-Bn-TE1PA** (Figure 1). This work is significant because theranostic approaches in HER2-positive gastric cancer using trastuzumab are rare, particularly with the copper-64/67 theranostic pair. The aim of the study was to develop a theranostic agent using **TE1PA** to chelate copper-64 for PET imaging and copper-67 for therapy. Pharmacological evaluations and proof-of-concept studies focused on HER2-positive gastric cancer using the NCI-N87 cell line.

EXPERIMENTAL SECTION

Material. Unless otherwise noted, all chemicals were purchased from commercial suppliers and were used without further purification. The bifunctional chelator ***p*-SCN-Bn-TE1PA**.3HCl was synthesized as previously described.[15] Trastuzumab (Herceptin®, Roche) was supplied by Oncodesign Services. Copper-64 was produced in Werner Siemens Imaging Center (Department of Preclinical Imaging and Radiopharmacy, University Hospital Tübingen, Tübingen, Germany) as $[^{64}Cu]CuCl_2$ in 0.1 M HCl. Copper-67 was purchased from Canadian Isotope Innovations Corp. (Saskatchewan Centre for Cyclotron Sciences, Saskatoon, Canada) as $[^{67}Cu]CuCl_2$ in 0.01 M HCl. Mouse experiments were conducted in licensed facilities and complied with European and national regulations. All experiments involving laboratory animals were performed in accordance with protocols approved by Oncodesign Services (Dijon, France) for tumor induction, the Werner Siemens Imaging Center (Tübingen, Germany) for biodistribution and imaging studies or by Bioemtech and NCSR "Demokritos" (Athens, Greece) for efficacy studies.

Analytical methods used for characterization and stability studies, including LC-MS, ITLC and SEC-HPLC, are reported in Supplementary information.

Bioconjugation. Detailed bioconjugation conditions are provided in Supplementary information. Briefly, trastuzumab in 0.3 M sodium carbonate-bicarbonate buffer (pH 8.6) was conjugated with 10-, 20- or 30-fold molar excess of ***p*-SCN-Bn-TE1PA** in water overnight at room temperature. After purification by size exclusion (PD10 column) and concentration by ultrafiltration (Amicon) in 0.1 M sodium acetate buffer (pH 6), the bioconjugate was characterized using UV-visible spectrometry to determine its concentration, SEC-HPLC to assess its purity, and mass spectrometry to quantity the number of chelators per antibody leading to degree of labeling (DOL).

Cancer cell lines. Cells were obtained from the ATCC (American Type Culture Collection, USA) including: *i)* HER2-positive NCI-N87 gastric carcinoma cell line, which was isolated from the stomach of a male gastric carcinoma patient;[17] *ii)* HER2 positive BT-474 human breast carcinoma cell line which was isolated from a solid, invasive ductal carcinoma of the breast from a 60-year-old Caucasian female patient (positive control);[18] and *iii)* HER2-negative MDA-MB-468 human breast carcinoma cell line, isolated in 1977 by R. Cailleau et al., from a pleural effusion of a 51-year-old black female patient with metastatic breast adenocarcinoma (negative control).[19]

The cell culture method is described in Supplementary information.

Binding assays and validation of HER2 expression. Binding assays of **Trastuzumab-*p*-SCN-Bn-TE1PA** on BT-474 cell line and HER2 expression on selected cell lines, NCI-N87, BT-474 (positive control) and MDA-MB-468 (negative control) were determined by flow cytometry. Staining was acquired on FACS performed with a FortessaX20 cytometer equipped with four excitation lasers (BD Biosciences). Data were analyzed using FlowJo software (Becton Dickinson). This method is described in the Supplementary information.

Radiolabeling. **Trastuzumab-*p*-SCN-Bn-TE1PA** (DOL of 2) was labeled with [^{64}Cu]$CuCl_2$ or [^{67}Cu]$CuCl_2$ in 0.5 M ammonium acetate buffer (pH 5.0-6.0) at 42 °C for 1 h. The stability of [^{64}Cu]Cu-**Trastuzumab-*p*-SCN-Bn-TE1PA** was determined at room temperature in 1X PBS (pH 7.4) after 4 h. The stability of [^{67}Cu]Cu-**Trastuzumab-*p*-SCN-Bn-TE1PA** was evaluated at room temperature in 1X PBS (pH 7.4), ascorbic acid, gentisic acid and DTPA solutions until 24 h. Details of the procedures are reported in Supplementary information.

Animal model. All *in vivo* studies were performed in female Swiss nude mice (Charles River Laboratories). The mice were 6-8 weeks old and received a subcutaneous injection into the right flank of $1x10^7$ NCI-N87 gastric carcinoma cells in 200 µL of cell culture medium containing 50% (v/v) matrigel. To improve cell engraftment, NCI-N87 tumor cell implantation was performed 72 h after whole-body irradiation with a gamma-source (2 Gy, 60Co, BioMep, France).

PET imaging. The ^{64}Cu-immunoconjugate was administered to mice (n = 10) by intravenous injection (IV) into the caudal at day 9 post tumor cell inoculation. Group 1 (n = 5): animals received a single injection of [^{64}Cu]Cu-**Trastuzumab-p-SCN-Bn-TE1PA** 10 MBq. Group 2 (n = 5): animals received a single co-injection of [^{64}Cu]Cu-**Trastuzumab-p-SCN-Bn-TE1PA** 10 MBq and 2000 µg of trastuzumab (see Supplementary information). PET imaging was performed on 3 mice from each group at 2, 24 and 48 h under isoflurane anesthesia (Inveon, Siemens Preclinical Solutions) and images were followed by MR scan (BioSpec, Bruker BioSpin GmbH). Biodistribution from PET image processing was performed on several organs including the tumor, kidneys, spleen and liver (see Supplementary information).

***Ex vivo* biodistribution**. All mice from each group were euthanized at 48 h, immediately after the last PET image acquisition. Samples were collected: tumor, blood, kidneys, liver, muscle, stomach, colon, heart, spleen and tail. Retrobulbar blood collection was conducted as a terminal procedure under deep isoflurane gas anesthesia. Samples activity was determined with a gamma counter (WIZARD24800010, Perkin-Elmer Inc.), see Supplementary information.

Therapeutic study. The preparation of trastuzumab (Herceptin®) is reported in Supplementary information. In this therapy experiment**,** mice (n = 40) were injected *via* IV into the caudal vein on day 9 post cell inoculation. Group 1 (n = 10): animals received a single injection of the vehicle (1X PBS solution at pH 7.4, 10 mL/kg); group 2 (n = 10): animals received a single injection of [^{67}Cu]Cu-**Trastuzumab-*p*-SCN-Bn-TE1PA** 10 MBq; group 3 (n = 10): animals received a single injection of [^{67}Cu]Cu-**Trastuzumab-*p*-SCN-Bn-TE1PA** 20 MBq; group 4 (n = 10): animals received the standard of care treatment, i.e. trastuzumab, twice a week for three weeks (5 mL/kg). Mice were euthanized once their tumor volume exceeded 1500 mm^3, or at 80 days after treatment, or when 20% of body weight loss was observed, or if there were other signs of pain, suffering or distress.

Body weight change (BWC) and efficacy parameters including tumor volume, tumor growth inhibition and tumor growth delay were determined and details can be found in Supplementary information.

The toxicity was evaluated by collecting blood samples from mice for each group after euthanasia and plasma was prepared to be analyzed for the following parameters: AST (aspartate aminotransferase), ALT (alanine aminotransferase), TBIL (bilirubin), CRE (creatinine) and ALB (albumin).

Statistical analysis. Data were analyzed using GraphPad Prism® (GraphPad Prism Software, USA). Comparisons were performed with ANOVA. A p value ≤ 0.05 was considered significant. If significant, pairwise tests were performed using the Bonferroni correction or with Tukey's multiple comparison or with log-rank (Mantel-Cox) test. In order to control for multiple comparisons, the p value was adjusted (p_{adj}). Data are presented as mean, standard deviation, standard error of the mean (SEM), median, and range.

RESULTS

Bioconjugation. *p*-SCN-Bn-TE1PA (10, 20 or 30 equivalents) was successfully conjugated to trastuzumab antibody with DOLs between 1.1 and 2.0 (Table S1), assessed by mass spectrometry. The DOL increased only slightly with the amount of ***p*-SCN-Bn-TE1PA** used (Figure S1). The two-fold labeled antibody variant increased from 21% for 10 equivalents of chelator to 28% for both 20 and 30 equivalents, while the fraction of the unlabeled antibody decreased from 33% to 17% and 11%, respectively. The overall yields for **Trastuzumab-*p*-SCN-Bn-TE1PA** were consistently high, ranging from 90 to 99%. SEC-HPLC analysis confirmed the absence of aggregates under all conditions (Figure S2), and the purity of the conjugates exceeded 95% (96.8, 96.4 and 95.9% for DOL values of 1.1, 1.7 and 2.0, respectively).

Binding assays. The cellular uptake of **Trastuzumab-*p*-SCN-Bn-TE1PA** was evaluated *via* flow cytometry binding assays on BT-474 cells using three test batches with different DOLs. Non-conjugated trastuzumab served as the positive control, while the isotype (IgG1) was used as the negative control. No significant difference in cellular uptake was observed between the bioconjugates and non-conjugated trastuzumab, whatever the DOL (Figure 2).

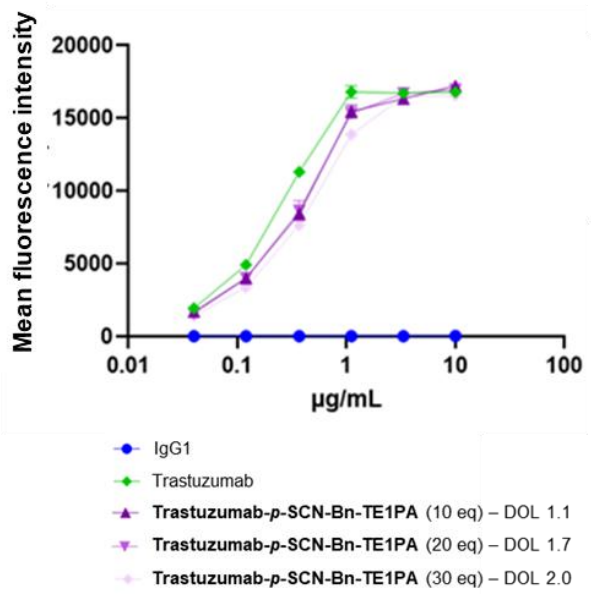

Figure 2. Evaluation of cellular uptake of **Trastuzumab-p-SCN-Bn-TE1PA** on BT 474 cells by flow cytometry.

Radiolabeling. Trastuzumab-*p*-SCN-Bn-TE1PA (DOL of 2) was successfully radiolabeled with [^{64}Cu]$CuCl_2$ or [^{67}Cu]$CuCl_2$ in 0.5 M ammonium acetate buffer (pH 5.0-6.0) at 42 °C for 1 h. [^{64}Cu]Cu-**Trastuzumab-*p*-SCN-Bn-TE1PA** was isolated with purities of 95% and 94%, as measured by ITLC and SEC-HPLC, respectively (Figure S3). For [^{67}Cu]Cu-**Trastuzumab-*p*-SCN-Bn-TE1PA**, two solutions were prepared, radiochemical purity exceeded 98% as confirmed by ITLC and SEC HPLC analysis, and final activity was 0.110 MBq/µg (Figure. S4 and S5).

Stability study. Stability of [^{64}Cu]Cu-**Trastuzumab-*p*-SCN-Bn-TE1PA** was evaluated in 1X PBS (pH 7.4) after 4 h, with radiochemical purities of 89% by ITLC and 81% by SEC-HPLC (Figure S6). Stability of [^{67}Cu]Cu-**Trastuzumab-*p*-SCN-Bn-TE1PA** was further assessed *via* ITLC at 0, 2, 4 and 24 h at room temperature in four different media: *i)* 1X PBS (pH 7.4), *ii)* ascorbic acid (5 mg/mL), *iii)* gentisic acid (5 mg/mL), and *iv)* 2000-fold molar excess of DTPA. (Figure S7). Radiochemical purity remained essentially unchanged in ascorbic acid, while a slight decrease was observed in PBS and gentisic acid (~85% at 24 h). In the presence of DTPA, a more significant drop to ~75% was observed, reflecting partial transchelation. These results confirm the overall good kinetic inertness of the radiocomplex under physiological and mildly challenging conditions.

Validation of HER2 expression. HER2 expression on selected cell lines (NCI-N87, BT-474 and MDA-MB-468) was quantified by flow cytometry (Figure 3). BT-474 breast cancer cells exhibited the highest HER2 expression with mean fluorescent intensity (MFI) of 32564, followed by NCI-N87 gastric cancer cells with MFI of 24104. In contrast, MDA-MB-468 cells showed negligible HER2 expression with MFI of 46. Representative histograms are provided in Figure S8.

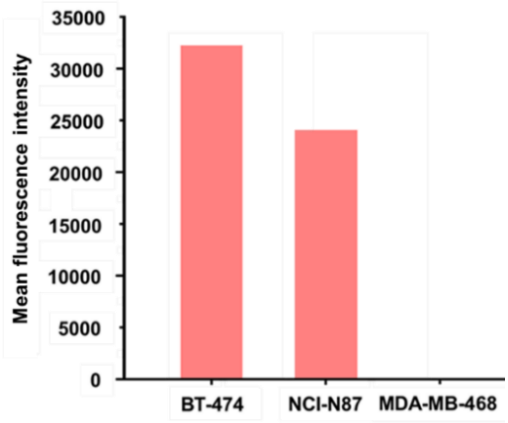

Figure 3. HER2 expression levels in NCI-N87, BT-474 and MDA-MB-468 cell lines measured by flow cytometry.

PET imaging. Mice bearing subcutaneous NCI-N87 tumors were injected with 10 MBq of [^{64}Cu]Cu-**Trastuzumab-*p*-SCN-Bn-TE1PA** alone (group 1, n = 5) or co-injected with an excess of unlabeled trastuzumab (group 2, n = 5). Representative PET images for both groups at 2, 24 and 48 h post-administration are shown in Figure 4A, while all individual images are provided in Figure S9 and S10. The images clearly showed notably higher activity in the tumor for [^{64}Cu]Cu-**Trastuzumab-*p*-SCN-Bn-TE1PA** (group 1) compared to the blocking group, where the excess of trastuzumab reduced tumor uptake. In contrast, uptake in normal organs, including the liver and spleen, appeared similar for both groups (Figure 4A).

Quantification analysis of tumor, kidneys, spleen and liver images, at each time for groups 1 and 2, is displayed in Figure 4B, with corresponding data detailed in Table S2. Results showed a significant decrease in uptake of [^{64}Cu]Cu-**Trastuzumab-*p*-SCN-Bn-TE1PA** (group 1) in the liver, spleen and kidneys between 2 and 24 h post-injection. Specifically, the mean percentage of injected activity per cm^3 (%IA/cm^3) in the liver decreased from 9.43 ± 2.25 at 2 h to 6.47 ± 0.61 at 24 h. The uptake declined from 5.13 ± 0.81 to 3.70 ± 0.53 in the spleen and from 4.47 ± 0.67 to 3.00 ± 0.30 in the kidneys over the same period. [^{64}Cu]Cu-**Trastuzumab-*p*-SCN-Bn-TE1PA** uptake decreased slightly between 24 and 48 h, with mean %IA/cm^3 values at 48 h of 5.43 ± 0.74 in the liver, 3.43 ± 0.85 in the spleen and 2.53 ± 0.25 in the kidneys. In contrast, tumor uptake increased over time with mean %IA/cm^3 rising from 2.07 ± 0.42 at 2 h, to 8.20 ± 1.21 at 24 h, and further to 11.10 ± 0.92 at 48 h. As anticipated, tumor uptake in group 2, which received a blocking dose of trastuzumab, was significantly lower than in group 1. Mean %IA/cm^3 values were reduced by 1.77 ± 0.12 at 2 h, 3.50 ± 0.52 at 24 h, and 3.77 ± 0.68 at 48 h. These results suggest that the tumor uptake was specific. In contrast, the uptake in normal organs with an excess of trastuzumab (group 2) was similar to the values observed in group 1, suggesting a non-specific uptake in healthy tissues (Table S2).

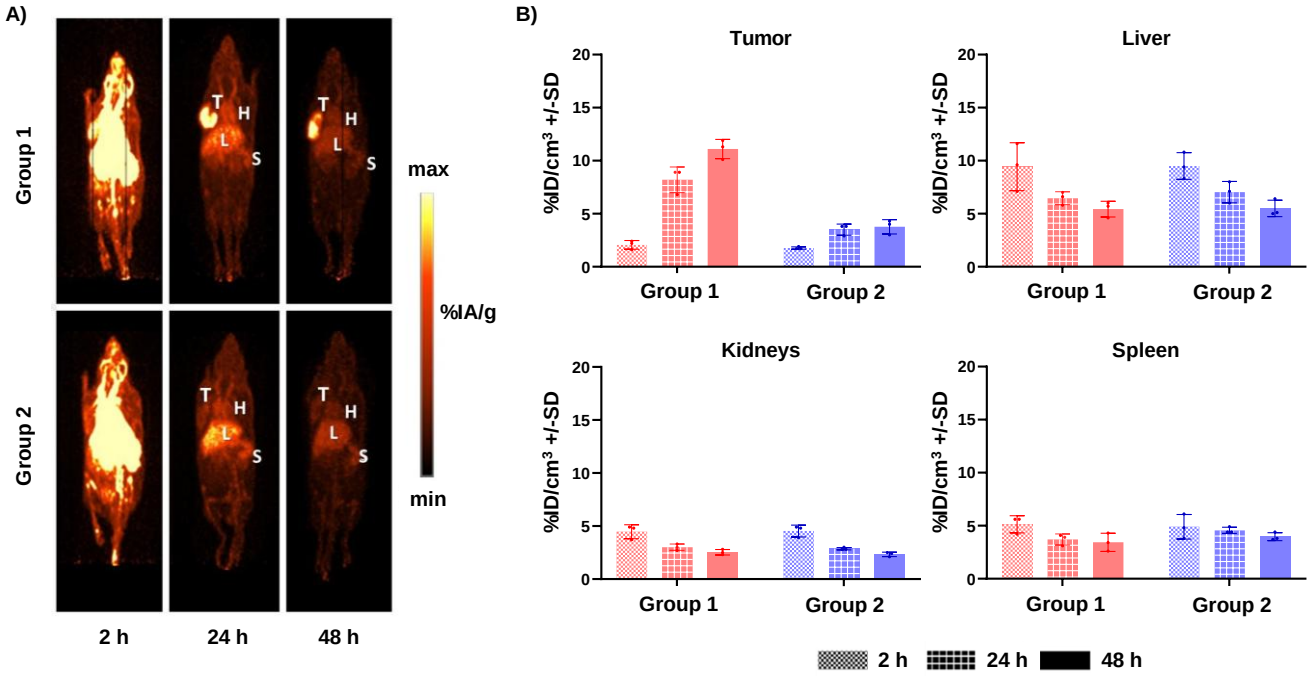

Figure 4. *In vivo* PET imaging of Swiss nude mice bearing subcutaneous NCI-N87 tumors at 2, 24 and 48 h post-injection. **A**) Representative images for group 1 ([^{64}Cu]Cu-**Trastuzumab-*p*-SCN-Bn-TE1PA,** n = 3) and group 2 ([^{64}Cu]Cu-**Trastuzumab-*p*-SCN-Bn TE1PA** + trastuzumab (blocking, n=3). Abbreviations: T = tumor, H = heart, L = liver, S = spleen. **B**) Quantitative analysis of [^{64}Cu]Cu-**Trastuzumab-*p*-SCN-Bn-TE1PA** uptake (n = 3 for each group, mean ± SD).

***Ex vivo* biodistribution.** After the last image acquisition (48 h), animals were euthanized and organs were collected. The percentage of the injected dose per gram of tissue (%IA/g) was determined to provide radioimmunoconjugate biodistribution profile (Figure 5 and Table S3).

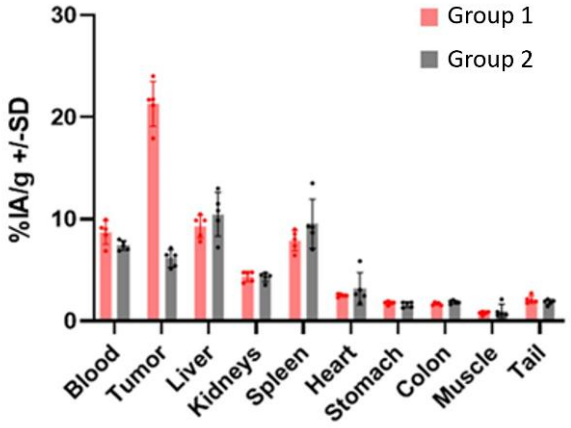

Figure 5. Biodistribution diagram of group 1 ([^{64}Cu]Cu-**Trastuzumab-*p*-SCN-Bn-TE1PA**) and group 2 ([^{64}Cu]Cu-**Trastuzumab-*p*-SCN-Bn TE1PA** + trastuzumab (blocking) in Swiss nude mice bearing subcutaneous NCI-N87 tumors. Animals were euthanized at 48 h.

For [^{64}Cu]Cu-**Trastuzumab-*p*-SCN-Bn-TE1PA** (group 1), data at 48 h post-injection revealed a significant activity in the tumor of 21.33 ± 2.19 %IA/g, markedly superior to that in all other organs. Among normal tissues, the highest uptake was observed in the spleen (7.89 ± 1.01 %IA/g), liver (9.30 ± 1.12 %IA/g) and kidneys (4.39 ± 0.50 %IA/g). The mean uptake in the blood was of 8.70 ± 1.15 %IA/g. Levels of activity in the heart, stomach and colon ranged from 1.7 to 2.5 %IA/g (2.54 ± 0.13, 1.79 ± 0.16 and 1.71 ± 0.12 %IA/g, respectively). Muscle tissue exhibited the lowest uptake with a mean value of 0.81 ± 0.18 %IA/g.

The tumor uptake decreased drastically with excess trastuzumab (group 2) with a lower mean %IA/g of 6.14 ± 0.85 compared with 21.33 ± 3.84 for group 1. As previously reported, these results confirmed specific uptake in the tumor. For group 2, uptake into the blood was slightly lower with a mean %IA/g of 7.43 ± 0.46 compared with 8.70 ± 1.15 for group 1. In contrast, uptake in normal organs in the presence of excess trastuzumab was slightly higher in the spleen (9.55 ± 2.40 %IA/g) and liver (10.50 ± 2.15 %IA/g) compared with group 1 (7.89 ± 1.01 %IA/g and 9.30 ± 1.12 %IA/g, respectively). For the other organs, biodistribution was similar.

Therapeutic Study. Therapy experiments were conducted in the NCI-N87 mouse model, as previously described. Two groups received a single injection of [67Cu]Cu-Trastuzumab-p-SCN-Bn-TE1PA at different doses of 10 MBq (group 2, n = 10) and 20 MBq (group 3, n = 10). A control group received the vehicle at 10 mL/kg (group 1, n = 10), while the last group received repeated doses of trastuzumab at 5 mL/kg (group 4, n = 10) to assess the effect of immunotherapy treatment. The antitumoral activity of [^{67}Cu]Cu-Trastuzumab-p-**SCN-Bn-TE1PA** was assessed by monitoring tumor volume, allowing evaluation of tumor growth delay and inhibition compared with vehicle (group 1) and trastuzumab (group 4). Individual tumor volume

curves for each group are shown in Figure 6A, while mean tumor volume curves and comparative analyses on days 25, 36 and 53 are provided in Figure S11 and S12, respectively.

At 25 days post-inoculation, mean tumor volume in mice treated with [^{67}Cu]Cu-**Trastuzumab-*p*-SCN-Bn-TE1PA** (262.6 ± 73.8 mm^3 using 20 MBq and 457.2 ± 146.5 mm^3 using 10 MBq) and trastuzumab (812.6 ± 217.9 mm^3) was significantly lower compared with the vehicle group (1190.0 ± 283.5 mm^3) ($p < 0.0001$ for groups 2 and 3; and $p = 0.0002$ for group 4). Although dose repetition of trastuzumab was used during the study, tumor volumes remained higher than in mice receiving ^{67}Cu-based radiotherapy. The difference in tumor volume between the two radioactive doses at day 25 was not statistically significant ($p = 0.1781$).

After 36 days, the mean tumor volume in mice treated with [^{67}Cu]Cu-**Trastuzumab-*p*-SCN-Bn-TE1PA** remained lower, with values of 627.3 ± 216.4 mm^3 for the 10 MBq dose and 286.7 ± 91.7 mm^3 for the 20 MBq dose, compared to the trastuzumab treated group, which exhibited a larger high tumor volume of 1103.0 ± 272.6 mm^3. These differences were statistically significant ($p < 0.0001$ for group 2 and 3 compared to group 4). Significant difference was also observed between the two radioactive doses ($p = 0.0005$).

At day 53, mice receiving a dose of 20 MBq of [^{67}Cu]Cu-**Trastuzumab-*p*-SCN-Bn-TE1PA** displayed a lower mean tumor volume of 775.9 ± 276.1 mm^3 compared to those receiving the 10 MBq dose, with a value of 1102.2 ± 392.8 mm^3. However, this difference was not statistically significant ($p = 0.1964$).

To evaluate the tumor growth delay, the mean time to reach the target tumor volume of 800 mm^3 was calculated for each group (Table S4 and Figure S13). Results showed a significant delay in tumor growth in mice treated with [^{67}Cu]Cu-**Trastuzumab-*p*-SCN-Bn-TE1PA** (10 or 20 MBq) compared to the vehicle and trastuzumab treatments. The mean time to reach 800 mm^3 was 43 ± 18 days for the 10 MBq dose (group 2) and 58 ± 11 days for the 20 MBq dose (group 3), versus 25 ± 8 days for the trastuzumab treated group ($p = 0.0046$ for group 2; $p < 0.0001$ for group 3). Group 4 showed slightly longer value compared to the vehicle (18 ± 3 days) but this difference was not significant ($p > 0.9999$).

Tumor growth inhibition was determined by comparing the median tumor volume of the treated groups 2, 3 and 4 to the vehicle (group 1) (Table S5). At 29 days post-administration, [^{67}Cu]Cu-**Trastuzumab-*p*-SCN-Bn-TE1PA** (10 MBq) displayed a moderately high tumor growth inhibition with an optimal value of 67%. Radiotherapy using the 20 MBq dose led to a high tumor growth inhibition with optimal value of 81%. Trastuzumab treatment exhibited a very moderate value of 36%.

The efficiency of the ^{67}Cu-radiotherapy was clearly demonstrated through Kaplan–Meier curves (Figure 6B). The median survival times for the vehicle group (31 days) and trastuzumab group (41 days) were significantly lower than those observed in groups receiving radioimmunotherapy. Specifically, the groups treated with [^{67}Cu]Cu-**Trastuzumab-*p*-SCN-Bn-TE1PA** showed extended median survival time of 60 days with 10 MBq and 74 days with 20 MBq. Statistical analysis confirmed significant differences between the vehicle and all treatment groups, though no statistically significant differences were found between the 10 and 20 MBq radiotherapy doses.

The potential toxicity of all treatments was evaluated by monitoring body weight at least twice a week for each animal, as well as through plasma analyses performed at the time of sacrifice across the different groups. All treatments were generally well tolerated, with only a transient body weight reduction

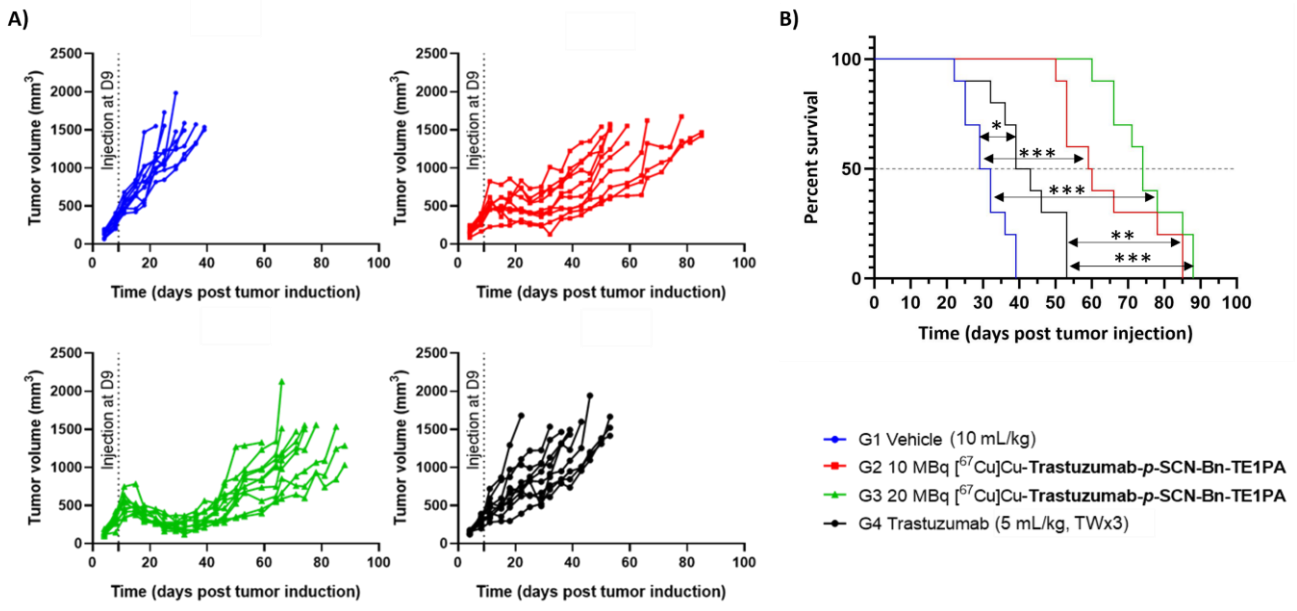

Figure 6. A) Individual tumor volume curves of Swiss nude mice bearing subcutaneous NCI-N87 tumors when treated with [^{67}Cu]Cu-**Trastuzumab-*p*-SCN-Bn-TE1PA** 10 and 20 MBq, vehicle and trastuzumab. **B**) Kaplan–Meier plot representing the survival of the mice of each group. Median survivals: 31 days (vehicle; blue), 41 days (trastuzumab; red), 60 days (10 MBq of [^{67}Cu]Cu-**Trastuzumab-*p*-SCN-Bn-TE1PA**; green) and 74 days (20 MBq of [^{67}Cu]Cu-**Trastuzumab-*p*-SCN-Bn-TE1PA**; black). Statistical analyses were carried out with log-rank (Mantel–Cox) test with (*) $p = 0.0056$, (**) $p = 0.0005$ and (***) $p < 0.0001$.

observed in the groups treated with [^{67}Cu]Cu-**Trastuzumab-*p*-SCN-Bn-TE1PA** during the first few days after injection. The body weight loss was minimal (< 5%) and self-corrected shortly thereafter (Figure S14 and S15). No body weight loss requiring clinical intervention or reaching ethical limits was observed. All animals were sacrificed once their tumor volume exceeded 1500 mm^3 or at the end of the study. Toxicity was evaluated by measuring levels of aspartate transaminase (AST), alanine transaminase (ALT), total bilirubin (TBIL), creatinine (CRE) and albumin (ALB). Comparative analyses of the concentrations for each parameter were performed (Figure S16). Notably, for group 1, only three values for AST, ALT and TBIL, and five for the other parameters, were available. A slight increase in ALT levels was observed for [^{67}Cu]Cu-**Trastuzumab-*p*-SCN-Bn-TE1PA** for both doses (27.5 ± 4.6 IU/L for 10 MBq and 33.2 ± 5.1 IU/L for 20 MBq) compared to the vehicle (20.3 ± 4.2 IU/L) and trastuzumab treatment (21.0 ± 3.7 IU/L) suggesting mild liver toxicity. The difference between the vehicle and group 2 (10 MBq) was not statistically significant (p = 0.2901) while group 3 (20 MBq) showed a significant difference with the vehicle (p = 0.0051).

AST and TBIL concentrations decreased in the radioactive treated groups (group 2 and 3) compared to the vehicle and trastuzumab, these differences were not statistically significant. CRE level, a marker of renal toxicity, showed no significant differences between groups except between group 2 and trastuzumab treated group (0.056 ± 0.030 mg/dL and 0.114 ± 0.053 mg/dL, respectively) (p = 0.0049). [^{67}Cu]Cu-**Trastuzumab-*p*-SCN-Bn-TE1PA** at 10 or 20 MBq doses displayed slightly lower concentrations (0.056 ± 0.030 mg/dL and 0.076 ± 0.034 mg/dL, respectively) with not significant difference compared to the vehicle (p = 0.2130 for group 2 and 0.8317 for group 3). The ALB concentration data showed statistically significant differences between the control group and both [^{67}Cu]Cu-**Trastuzumab-*p*-SCN-Bn-TE1PA** groups (p < 0.01), as well as between trastuzumab treatment and both radiotherapy groups (p < 0.005) with concentration values ranged from 1.92 ± 0.06 g/dL to 2.22 ± 0.08 g/dL.

DISCUSSION

HER2-positive gastric cancer is a highly aggressive disease, characterized by rapid growth, significant heterogeneity, and poor prognosis. This highlights the urgent need for effective imaging probes to facilitate accurate diagnosis and guide treatment decisions. Despite the critical nature of this issue, only a limited number of studies have investigated nuclear medicine approaches for both imaging and therapy of gastric cancers.[20–24] Considering the growing recognition of HER2 overexpression in gastric cancer patients, our research focused on using trastuzumab to target the NCI-N87 human gastric adenocarcinoma cell line. Notably, radiolabeled trastuzumab compounds for gastric cancer remain scarce, especially those incorporating copper radioisotopes.[23,25,26] The recent increased availability of copper-67, made possible by advancements in its production at a sufficient quantity and quality, opens new avenues for research and clinical applications.

In our previous work, we demonstrated the relevance ***p*-SCN-Bn-TE1PA** in the design of radiopharmaceuticals for ^{64}Cu-PET imaging[15,16] or even ^{64}Cu-based therapy.[27] Other chelating agents forming stable Cu(II) complexes *in vivo* have been reported in the literature, such as CB-TE1PA which requires drastic radiolabeling conditions limiting radiopharmaceutical applications, or sarcophagin (Sar) which is currently the subject of a clinical study using the ^{64}Cu/^{67}Cu pair.[28–30] The development of highly stable copper chelators based on TE1PA has further increased interest in copper-67 as a therapeutic radionuclide. Based on these findings, we have developed a novel theranostic radiopharmaceutical featuring a unique bioconjugate capable of being labeled with copper-64 for PET imaging, and copper-67 for therapeutic applications.

The bioconjugation of trastuzumab with ***p*-SCN-Bn-TE1PA** was highly efficient, with 1.1 to 2.0 ligands coupled per antibody using 10 to 30 equivalents of ligand, without any loss in binding affinity compared to unconjugated trastuzumab. In this study, we aimed for an average DOL close to 2, a value considered sufficient for efficient radiolabeling while preserving antibody integrity. Notably, under the same mild conjugation conditions, some bifunctional chelators have been reported to yield higher DOL values, suggesting that structural features such as size and accessibility may influence labeling efficiency. The confirmed high HER2 expression in the NCI-N87 cell line allowed the development of a mouse model of gastric cancer. Successful radiolabeling with copper-64 enabled a biodistribution study of [^{64}Cu]Cu-**Trastuzumab-*p*-SCN-Bn-TE1PA** (DOL of 2.0) for immuno-PET imaging of gastric cancer. The specific targeting of HER2-expressing tumors was clearly highlighted on PET images with high contrast using a blocking group.

Tumor-to-liver ratios at 24 and 48 h using [^{64}Cu]Cu-**Trastuzumab-*p*-SCN-Bn-TE1PA** were notably higher (1.27 and 2.04, respectively) than those observed with co-injection of trastuzumab (0.50 and 0.69, respectively) (Table S2). This indicated a faster hepatic clearance of the radiotracer with the blocking group, supporting the effective tumor targeting of [^{64}Cu]Cu-**Trastuzumab-*p*-SCN-Bn-TE1PA**. *Ex vivo* biodistribution results further confirmed the specific binding of the radio-immunoconjugate to the tumor, with reduced tumor uptake observed in the group receiving an excess of trastuzumab (group 2), emphasizing its potential for targeted therapy. Blood-to-muscle ratios (~11 for group 1 and ~7 for group 2) (Table S3) suggested that a small amount of activity remained in the bloodstream at 48 h, expected with the long biological half-life of antibodies. The liver uptake in both groups was comparable (liver-to-muscle ratio of around 11). However, tumor accumulation differed significantly, as expected, with the tumor-to-muscle ratio in group 1 being more than four times higher, around 26, *vs* 6 for group 2. The tumor-to-liver ratio for [^{64}Cu]Cu-**Trastuzumab-*p*-SCN-Bn-TE1PA** was approximately 2, while the blocking dose showed a ratio of 0.6, indicating that, after 48 h, the liver accumulated nearly twice as much of the compound than the tumor. These tumor-to-liver ratios were consistent with those calculated from PET image analysis (Table S2). Our ^{64}Cu-PET study underscored the promising application of [^{64}Cu]Cu-**Trastuzumab-*p*-SCN-Bn-TE1PA** as a radiotracer in the field of molecular imaging, providing a valuable tool for diagnosis of HER2-positive tumors and monitoring trastuzumab-targeted radiotherapy. Although studies focusing on the identification of HER2-positive tumors using ^{64}Cu-PET imaging are limited, examples of ^{64}Cu-trastuzumab conjugates using DOTA or NOTA chelators have been reported. [^{64}Cu]Cu-**Trastuzumab-DOTA** has been studied in both HER2-positive breast and gastric cancers.[25,31,32] As well-documented for ^{64}Cu-DOTA-based radiopharmaceuticals,[28] this radiotracer exhibited high liver uptake, likely due to hepatic metabolism and copper-64 transchelation. The use of NOTA

improved stability in the liver, especially compared with DOTA which showed significant *in vivo* dissociation, leading to increased hepatic accumulation of free copper, likely due to transchelation to proteins such as superoxide dismutase (SOD).[33] In our previous studies, we observed similar results, demonstrating that TE1PA offers superior ^{64}Cu-nuclide coordination properties compared to DOTA and NOTA chelators.[16]

Focusing on a theranostic approach using a chemically identical bioconjugate, we studied **Trastuzumab-*p*-SCN-Bn-TE1PA** labeled with copper-67 to assess its therapeutic potential in the same murine model of gastric cancer. The therapeutic study of [^{67}Cu]Cu-**Trastuzumab-*p*-SCN-Bn-TE1PA** in NCI-N87 subcutaneously grafted mice demonstrated a significant enhancement in anti-tumor activity at doses of 10 and 20 MBq, compared to the vehicle (group 1) and standard trastuzumab treatment (group 4). This was evidenced by notably reduced tumor growth (Figure 6A and Figure S11) and increased median survival time (Figure 6B), highlighting its potential as a promising therapeutic agent.

The observed anti-tumor effects were primarily attributed to the β^- ionizing emission of copper-67, as the efficacy of [^{67}Cu]Cu-**Trastuzumab-*p*-SCN-Bn-TE1PA** did not appear to be due to the antibody itself. Indeed, a limited effect on tumor growth delay was observed in group 4, which received standard trastuzumab treatment (two injections per week for three weeks). This was further confirmed by the increase in tumor size in the vehicle group (group 1) throughout the study, while groups 2 and 3, which received [^{67}Cu]Cu-**Trastuzumab-*p*-SCN-Bn-TE1PA**, showed a clear trend toward tumor growth inhibition.

A dose-dependent response was observed, with more effective tumor-growth inhibition and improved median survival at the higher dose of 20 MBq of [^{67}Cu]Cu-**Trastuzumab-*p*-SCN-Bn-TE1PA.** Indeed, a clear reduction in the tumor size was observed for group 3 almost immediately after injection, while group 2 displayed minimal changes in the tumor size until 32 days post-injection. Thus, treatment with [^{67}Cu]Cu-**Trastuzumab-*p*-SCN-Bn-TE1PA**, whether with 10 or 20 MBq doses, exhibited a significantly greater anti-tumor effect than trastuzumab alone, reinforcing the efficacy of targeted radiotherapy for HER2-positive tumors.

The therapeutic efficiency demonstrated in this study was accompanied by no significant toxicity and good tolerance of each treatment. Comparative analyses of clinical biochemistry parameters at the end of the study showed, in general, no significant differences between group 1 (vehicle) and group 4 (trastuzumab), or between the groups treated with copper-67 (Figure S16). A slight but statistically significant increase in ALT levels was observed in group 3 (20 MBq), with no corresponding elevations in AST, TBIL, or CRE. These findings may suggest a limited hepatic impact at higher doses of [^{67}Cu]Cu-Trastuzumab-***p*-SCN-Bn-TE1PA**, but remained within a range compatible with good overall tolerance.

CONCLUSIONS

Altogether, this study further supports the potential of ^{64}Cu/^{67}Cu-labeled trastuzumab conjugates for HER2-positive cancer theranostics, and illustrates that TE1PA-based bifunctional chelators constitute an additional valuable option among currently available systems such as NOTA and sarcophagine derivatives. In addition, the theranostic approach using the copper-64/copper-67 pair demonstrates significant potential for the treatment of gastric cancer by considering this new proof of concept. Our results underline the promising efficacy and safety of [^{67}Cu]Cu-**Trastuzumab-*p*-SCN-Bn-TE1PA** in improving treatment outcomes for HER2-positive gastric cancer, reinforcing its value in advancing precision oncology. This study demonstrates the success of an optimized combination: a single-element isotopic pair, a chelator with proven efficacy for copper chelation and radiolabeling, an accessible biological vector, and a therapeutically relevant target, namely gastric cancer, known for its demanding specificity. This work underscores the importance of chelator design in maximizing the potential of the copper-64/copper-67 pair for clinical applications, offering a compelling alternative to other radioisotopes in nuclear medicine.

ASSOCIATED CONTENT

Supporting Information. Materials and procedures for bioconjugation, binding assays, radiolabeling with ^{64}Cu- and ^{67}Cu-nuclides, HER2 expression validation and *in vivo* studies, analytical characterization of bioconjugates including mass spectra, SEC-HPLC, radioimmunoconjugates characterization including ITLC, SEC-HPLC and stability data, representative histograms for HER2 expression analysis, individual PET images at 2, 24 and 48 h, tables of PET analysis data and *ex vivo* biodistribution data, graphs of the therapeutic study with mean tumor volume curves, tumor volume on D25, D36 and D53, growth rates, tumor growth inhibition, individual body weight curves, mean body weight change curves and clinical biochemical parameters. [redacted]

AUTHOR INFORMATION

Corresponding Authors

* raphael.tripier@univ-brest.fr
* nathalie.lebris@univ-brest.fr

Author Contributions

Julie Pineau and Cédric Ollier performed the compound synthesis. Céline Mothes supervised laboratories and platforms, and analyzed results for the bioconjugation, radiochemistry, and *in vitro* analysis studies. Céline Mothes and Sarah Belderbos jointly managed the laboratories and platforms, and analyzed results for the *in vivo* experiments. Together, they prepared all graphical materials. Raphaël Tripier and Nathalie Le Bris managed and coordinated the study, designed the radiopharmaceutical, developed the methodology, and drafted the initial manuscript, with contributions from Julie Pineau. All authors reviewed and approved the final version of the manuscript.

Funding Sources

This study has been founded by the SATT Ouest Valorisation.

ACKNOWLEDGMENT

The authors would like to thank SATT Ouest Valorisation and Jean-Marc Herbert for their support. They also acknowledge Oncodesign, the Ligue contre le Cancer, the Brittany Region, the Ministère de l'Enseignement Supérieur de la Recherche, the Centre National de la Recherche Scientifique and the scientific facilities of the University of Brest.

REFERENCES

(1) Iqbal, N.; Iqbal, N. Human Epidermal Growth Factor Receptor 2 (HER2) in Cancers: Overexpression and Therapeutic Implications. *Mol. Biol. Int.* **2014**, *2014*, 852748. https://doi.org/10.1155/2014/852748.

(2) Abrahao-Machado, L. F.; Scapulatempo-Neto, C. HER2 Testing in Gastric Cancer: An Update. *World J. Gastroenterol.* **2016**, *22* (19), 4619. https://doi.org/10.3748/wjg.v22.i19.4619.

(3) Tabernero, J.; Hoff, P. M.; Shen, L.; Ohtsu, A.; Shah, M. A.; Siddiqui, A.; Heeson, S.; Kiermaier, A.; Macharia, H.; Restuccia, E.; Kang, Y.-K. Pertuzumab, Trastuzumab, and Chemotherapy in HER2-Positive Gastric/Gastroesophageal Junction Cancer: End-of-Study Analysis of the JACOB Phase III Randomized Clinical Trial. *Gastric Cancer* **2022**, *26* (1), 123. https://doi.org/10.1007/s10120-022-01335-4.

(4) Crișan, G.; Moldovean-Cioroianu, N. S.; Timaru, D.-G.; Andrieș, G.; Căinap, C.; Chiș, V. Radiopharmaceuticals for PET and SPECT Imaging: A Literature Review over the Last Decade. *Int. J. Mol. Sci.* **2022**, *23* (9), 5023. https://doi.org/10.3390/ijms23095023.

(5) Morgan, K. A.; Rudd, S. E.; Noor, A.; Donnelly, P. S. Theranostic Nuclear Medicine with Gallium-68, Lutetium-177, Copper-64/67, Actinium-225, and Lead-212/203 Radionuclides. *Chem. Rev.* **2023**, *123* (20), 12004–12035. https://doi.org/10.1021/acs.chemrev.3c00456.

(6) Akhavanallaf, A.; Peterson, A. B.; Fitzpatrick, K.; Roseland, M.; Wong, K. K.; El-Naqa, I.; Zaidi, H.; Dewaraja, Y. K. The Predictive Value of Pretherapy [^{68}Ga]Ga-DOTA-TATE PET and Biomarkers in [^{177}Lu]Lu-PRRT Tumor Dosimetry. *Eur. J. Nucl. Med. Mol. Imaging* **2023**, *50* (10), 2984. https://doi.org/10.1007/s00259-023-06252-x.

(7) Das, S.; Al-Toubah, T.; El-Haddad, G.; Strosberg, J. ^{177}Lu-DOTATATE for the Treatment of Gastroenteropancreatic Neuroendocrine Tumors. *Expert Rev. Gastroenterol. Hepatol.* **2019**, *13* (11), 1023. https://doi.org/10.1080/17474124.2019.1685381.

(8) Keinänen, O.; Fung, K.; Brennan, J. M.; Zia, N.; Harris, M.; van Dam, E.; Biggin, C.; Hedt, A.; Stoner, J.; Donnelly, P. S.; Lewis, J. S.; Zeglis, B. M. Harnessing ^{64}Cu/^{67}Cu for a Theranostic Approach to Pretargeted Radioimmunotherapy. *PNAS* **2020**, *117* (45), 28316–28327. https://doi.org/10.1073/pnas.2009960117.

(9) Dearling, J. L. J.; van Dam, E. M.; Harris, M. J.; Packard, A. B. Detection and Therapy of Neuroblastoma Minimal Residual Disease Using [$^{64/67}$Cu]Cu-SARTATE in a Preclinical Model of Hepatic Metastases. *EJNMMI Res.* **2021**, *11* (1), 20. https://doi.org/10.1186/s13550-021-00763-0.

(10) Rudd, S. E.; Zuylekom, J. V.; Cullinane, C.; Blyth, B. J.; Donnelly, P. S. Potential Theranostics of Breast Cancer with Copper-64/67 Sarcophagine-Trastuzumab. *Chem. Sci.* **2025**, *16* (9), 3998–4005. https://doi.org/10.1039/D4SC06969B.

(11) Mou, L.; Martini, P.; Pupillo, G.; Cieszykowska, I.; Cutler, C. S.; Mikołajczak, R. ^{67}Cu Production Capabilities: A Mini Review. *Molecules* **2022**, *27* (5), 1501. https://doi.org/10.3390/molecules27051501.

(12) Pougoue Ketchemen, J.; Njotu, F. N.; Babeker, H.; Ahenkorah, S.; Tikum, A. F.; Nwangele, E.; Henning, N.; Cleeren, F.; Fonge, H. Effectiveness of [^{67}Cu]Cu-Trastuzumab as a Theranostic against HER2-Positive Breast Cancer. *Eur. J. Nucl. Med Mol Imaging* **2024**, *51* (7), 2070–2084. https://doi.org/10.1007/s00259-024-06648-3.

(13) Lima, L. M. P.; Esteban-Gómez, D.; Delgado, R.; Platas-Iglesias, C.; Tripier, R. Monopicolinate Cyclen and Cyclam Derivatives for Stable Copper(II) Complexation. *Inorg. Chem.* **2012**, *51* (12), 6916–6927. https://doi.org/10.1021/ic300784v.

(14) Frindel, M.; Camus, N.; Rauscher, A.; Bourgeois, M.; Alliot, C.; Barré, L.; Gestin, J.-F.; Tripier, R.; Faivre-Chauvet, A. Radiolabeling of HTE1PA: A New Monopicolinate Cyclam Derivative for Cu-64 Phenotypic Imaging. In Vitro and in Vivo Stability Studies in Mice. *Nucl. Med. Biol.* **2014**, *41*, e49–e57. https://doi.org/10.1016/j.nucmedbio.2013.12.009.

(15) Le Bihan, T.; Navarro, A.-S.; Le Bris, N.; Le Saëc, P.; Gouard, S.; Haddad, F.; Gestin, J.-F.; Chérel, M.; Faivre-Chauvet, A.; Tripier, R. Synthesis of *C*-Functionalized TE1PA and Comparison with Its Analogues. An Example of Bioconjugation on 9E7.4 mAb for Multiple Myeloma ^{64}Cu-PET Imaging. *Org. Biomol. Chem.* **2018**, *16* (23), 4261–4271. https://doi.org/10.1039/C8OB00499D.

(16) Navarro, A.-S.; Le Bihan, T.; Le Saëc, P.; Bris, N. L.; Bailly, C.; Saï-Maurel, C.; Bourgeois, M.; Chérel, M.; Tripier, R.; Faivre-Chauvet, A. TE1PA as Innovating Chelator for ^{64}Cu Immuno-TEP Imaging: A Comparative in Vivo Study with DOTA/NOTA by Conjugation on 9E7.4 mAb in a Syngeneic Multiple Myeloma Model. *Bioconjugate Chem.* **2019**, *30* (9), 2393–2403. https://doi.org/10.1021/acs.bioconjchem.9b00510.

(17) Park, J.-G.; Frucht, H.; LaRocca, R. V.; Bliss, D. P., Jr.; Kurita, Y.; Chen, T.-R.; Henslee, J. G.; Trepel, J. B.; Jensen, R. T.; Johnson, B. E.; Bang, Y.-J.; Kim, J.-P.; Gazdar, A. F. Characteristics of Cell Lines Established from Human Gastric Carcinoma. *Cancer Res.* **1990**, *50* (9), 2773–2780.

(18) Lasfargues, E. Y.; Coutinho, W. G.; Redfield, E. S. Isolation of Two Human Tumor Epithelial Cell Lines from Solid Breast Carcinomas. *J. Natl. Cancer Inst.* **1978**, *61* (4), 967–978.

(19) Cailleau, R.; Olivé, M.; Cruciger, Q. V. J. Long-Term Human Breast Carcinoma Cell Lines of Metastatic Origin: Preliminary Characterization. *In Vitro* **1978**, *14* (11), 911–915. https://doi.org/10.1007/BF02616120.

(20) Zhou, N.; Liu, C.; Guo, X.; Xu, Y.; Gong, J.; Qi, C.; Zhang, X.; Yang, M.; Zhu, H.; Shen, L.; Yang, Z. Impact of ^{68}Ga-NOTA-MAL-MZHER2 PET Imaging in Advanced Gastric Cancer Patients and Therapeutic Response Monitoring. *Eur. J. Nucl. Med. Mol. Imaging* **2021**, *48* (1), 161–175. https://doi.org/10.1007/s00259-020-04898-5.

(21) Guo, X.; Zhou, N.; Chen, Z.; Liu, T.; Xu, X.; Lei, X.; Shen, L.; Gao, J.; Yang, Z.; Zhu, H. Construction of ^{124}I-Trastuzumab for Noninvasive PET Imaging of HER2 Expression: From Patient-Derived Xenograft Models to Gastric Cancer Patients. *Gastric Cancer* **2020**, *23* (4), 614–626. https://doi.org/10.1007/s10120-019-01035-6.

(22) Orlova, A.; Wållberg, H.; Stone-Elander, S.; Tolmachev, V. On the Selection of a Tracer for PET Imaging of HER2-Expressing Tumors: Direct Comparison of a ^{124}I-Labeled Affibody Molecule and Trastuzumab in a Murine Xenograft Model. *J. Nucl. Med.* **2009**, *50* (3), 417–425. https://doi.org/10.2967/jnumed.108.057919.

(23) Guo, X.; Zhu, H.; Zhou, N.; Chen, Z.; Liu, T.; Liu, F.; Xu, X.; Jin, H.; Shen, L.; Gao, J.; Yang, Z. Noninvasive Detection of HER2 Expression in Gastric Cancer by ^{64}Cu-NOTA-Trastuzumab in PDX Mouse Model and in Patients. *Mol. Pharmaceutics* **2018**, *15* (11), 5174–5182. https://doi.org/10.1021/acs.molpharmaceut.8b00673.

(24) Janjigian, Y. Y.; Viola-Villegas, N.; Holland, J. P.; Divilov, V.; Carlin, S. D.; Gomes-DaGama, E. M.; Chiosis, G.; Carbonetti, G.; Stanchina, E. de; Lewis, J. S. Monitoring Afatinib Treatment in HER2-Positive Gastric Cancer with ^{18}F-FDG and ^{89}Zr-Trastuzumab PET. *J. Nucl. Med.* **2013**, *54* (6), 936–943. https://doi.org/10.2967/jnumed.112.110239.

(25) Hernandez, M. C.; Yazaki, P.; Mortimer, J. E.; Yamauchi, D.; Poku, E.; Park, J.; Frankel, P.; Kim, J.; Colcher, D. M.; Wong, J.; Fong, Y.; Shively, J.; Woo, Y. Pilot Study of HER2 Targeted ^{64}Cu-DOTA-Tagged PET Imaging in Gastric Cancer Patients. *Nucl Med Commun* **2023**, *44* (12), 1151–1155. https://doi.org/10.1097/MNM.0000000000001761.

(26) Simó, C.; Shmuel, S.; Vanover, A.; Pereira, P. M. R. [^{64}Cu]Cu-NOTA-Trastuzumab and [^{89}Zr]Zr-DFO-Trastuzumab in Xenografts with Varied HER2 Expression. *Mol. Pharm.* **2024**, *21* (12), 6311–6322. https://doi.org/10.1021/acs.molpharmaceut.4c00777.

(27) Métivier, C.; Le Saëc, P.; Gaschet, J.; Chauvet, C.; Marionneau-Lambot, S.; Hofgaard, P. O.; Bogen, B.; Pineau, J.; Le Bris, N.; Tripier, R.; Alliot, C.; Haddad, F.; Chérel, M.;

Chouin, N.; Faivre-Chauvet, A.; Rbah-Vidal, L. Preclinical Evaluation of a ^{64}Cu-Based Theranostic Approach in a Murine Model of Multiple Myeloma. *Pharmaceutics* **2023**, *15* (7), 1817. https://doi.org/10.3390/pharmaceutics15071817.

(28) Boswell, C. A.; Sun, X.; Niu, W.; Weisman, G. R.; Wong, E. H.; Rheingold, A. L.; Anderson, C. J. Comparative in Vivo Stability of Copper-64-Labeled Cross-Bridged and Conventional Tetraazamacrocyclic Complexes. *J. Med. Chem.* **2004**, *47* (6), 1465–1474. https://doi.org/10.1021/jm030383m.

(29) Hicks, R. J.; Jackson, P.; Kong, G.; Ware, R. E.; Hofman, M. S.; Pattison, D. A.; Akhurst, T. A.; Drummond, E.; Roselt, P.; Callahan, J.; Price, R.; Jeffery, C. M.; Hong, E.; Noonan, W.; Herschtal, A.; Hicks, L. J.; Hedt, A.; Harris, M.; Paterson, B. M.; Donnelly, P. S. ^{64}Cu-SARTATE PET Imaging of Patients with Neuroendocrine Tumors Demonstrates High Tumor Uptake and Retention, Potentially Allowing Prospective Dosimetry for Peptide Receptor Radionuclide Therapy. *J. Nucl. Med.* **2019**, *60* (6), 777–785. https://doi.org/10.2967/jnumed.118.217745.

(30) Nordquist, L.; Lengyelova, E.; Saltzstein, D.; Josephson, D.; Franklin, G.; Morrish, G.; Gervasio, O.; Parker, M.; Miller, R.; Shore, N. COBRA: Assessment of Safety and Efficacy of ^{64}Cu-SAR-bisPSMA in Patients with Biochemical Recurrence of Prostate Cancer Following Definitive Therapy. *J. Nucl. Med.* **2024**, *65* (supplement 2), 242291–242291.

(31) Tamura, K.; Kurihara, H.; Yonemori, K.; Tsuda, H.; Suzuki, J.; Kono, Y.; Honda, N.; Kodaira, M.; Yamamoto, H.; Yunokawa, M.; Shimizu, C.; Hasegawa, K.; Kanayama, Y.; Nozaki, S.; Kinoshita, T.; Wada, Y.; Tazawa, S.; Takahashi, K.; Watanabe, Y.; Fujiwara, Y. ^{64}Cu-DOTA-Trastuzumab PET Imaging in Patients with HER2-Positive Breast Cancer. *J. Nucl. Med.* **2013**, *54* (11), 1869–1875. https://doi.org/10.2967/jnumed.112.118612.

(32) Mortimer, J. E.; Bading, J. R.; Park, J. M.; Frankel, P. H.; Carroll, M. I.; Tran, T. T.; Poku, E. K.; Rockne, R. C.; Raubitschek, A. A.; Shively, J. E.; Colcher, D. M. Tumor Uptake of ^{64}Cu-DOTA-Trastuzumab in Patients with Metastatic Breast Cancer. *J. Nucl. Med.* **2018**, *59* (1), 38–43. https://doi.org/10.2967/jnumed.117.193888.

(33) Woo, S.-K.; Jang, S. J.; Seo, M.-J.; Park, J. H.; Kim, B. S.; Kim, E. J.; Lee, Y. J.; Lee, T. S.; An, G. I.; Song, I. H.; Seo, Y.; Kim, K. I.; Kang, J. H. Development of ^{64}Cu-NOTA-Trastuzumab for HER2 Targeting: A Radiopharmaceutical with Improved Pharmacokinetics for Human Studies. *J. Nucl. Med.* **2019**, *60* (1), 26–33. https://doi.org/10.2967/jnumed.118.210294.

For Table of Contents Only

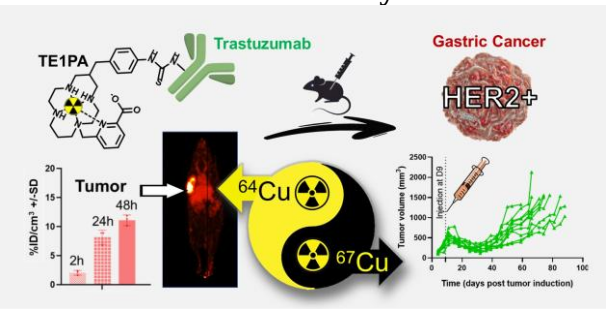

A copper-based theranostic approach combining $^{64}Cu/^{67}Cu$ isotopes with trastuzumab modified with TE1PA offers effective PET imaging, targeted radiotherapy, and high tumor specificity for HER2-positive gastric cancer, with minimal toxicity and strong therapeutic potential.